JBC RESEARCH ARTICLE

Homeodomain-interacting protein kinase HIPK4 regulates phosphorylation of manchette protein RIMBP3 during spermiogenesis

Received for publication, February 12, 2022, and in revised form, July 21, 2022 Published, Papers in Press, August 2, 2022,
https://doi.org/10.1016/j.jbc.2022.102327

Xiaofei Liu[1,‡], Chunyan Zang[1,‡], Yifei Wu[1,‡], Ru Meng[1,‡], Yu Chen[1], Tao Jiang[1], Cheng Wang[1], Xiaoyu Yang[2], Yueshuai Guo[1], Chenghao Situ[1], Zhibin Hu[1,*], Jun Zhang[1,*], and Xuejiang Guo[1,*]

From the [1]State Key Laboratory of Reproductive Medicine, Nanjing Medical University, Nanjing, China; [2]Center of Reproductive Medicine, First Affiliated Hospital of Nanjing Medical University, Nanjing, China

Edited by Qi-Qun Tang

Nonobstructive azoospermia (NOA) is the most serious form of spermatogenesis abnormalities in male infertility. Genetic factors are important to consider as elements leading to NOA. Although many pathogenic genes have been reported, the causative genes of NOA for many patients are still unknown. In this study, we found ten point mutations in the gene encoding homeodomain-interacting protein kinase 4 (HIPK4) in patients with NOA, and using *in vitro* studies, we determined a premature termination point mutation (p. Lys490*, c.1468A>T) that can cause decreased expression of HIPK4. Our phosphoproteomic analysis of *Hipk4*$^{-/-}$ testes revealed phosphorylation of multiple proteins regulated by HIPK4 during spermiogenesis. We also confirmed that a substrate of HIPK4 with four downregulated phosphorylation sites matching the xSPx motif is the known manchette-related protein RIMS-binding protein 3, which is required for sperm head morphogenesis. Therefore, we conclude HIPK4 regulates the phosphorylation of manchette protein RIMS-binding protein 3 and plays essential roles in sperm head shaping and male fertility.

Infertility is defined as the inability to conceive after 12 months of unprotected intercourse (1) and is a worldwide health problem affecting approximately 15% of couples (2). Male infertility often presents as oligoasthenoteratozoospermia (OAT) or the complete absence of sperm (azoospermia) in semen (3). Nonobstructive azoospermia (NOA) is the most severe phenotype of spermatogenesis abnormalities, accounting for about 60% of azoospermia according to Jarow *et al.* (4) and affecting about 10% of infertile men according to Matsumiya *et al.* (5). Although the etiology is known for some cases, the majority are idiopathic. Among the causes, genetic factors contribute to 21% to 29% of NOA (6), including chromosome number defects, Y-chromosome microdeletions, karyotype aberrations, and gene mutations (7). The identification of novel mutations in genes related to spermatogenesis is an important aspect of the diagnosis of the causes of infertility.

Spermatogenesis is a complex process, involves mitosis of spermatogonia, meiosis of spermatocytes, and spermiogenesis of spermatids to generate sperm (8, 9). During spermiogenesis, spermatids undergo dramatic morphological changes, including reshaping and condensation of the nucleus; removal of cytoplasm; and formation of mitochondrial sheath, acrosome, and flagella (10, 11). Many microtubule-based structures are involved in shaping the falciform spermatid head and assembly of the flagellum (12). Manchette is a transient microtubule and filamentous actin (F-actin)–containing structure, appears in spermatids at step 8 and disappears at around steps 13 to 14, and is critical for head shaping and flagellum formation (13). Manchette connects nucleus *via* two potential nucleation sites, the perinuclear ring, and the centrosome, with a "grass skirt-like" structure formed by parallel microtubule bundles (14), which is crucial for sperm head shaping. For example, deficiency of the spermatid nuclear membrane protein SUN4 led to a disconnection between the manchette microtubules and nuclear envelope, which caused round-headed sperm (15). While the absence of RIMS-binding protein 3 (RIMBP3), a manchette-associated protein, would lead to abnormal sperm head morphology and male infertility (16). However, the delicate function of manchette is under debate in terms of its role in spermatid head shaping and flagellum formation, and the molecular mechanisms and factors involved in this process remain poorly understood.

Protein phosphorylation is an important cellular regulatory mechanism. Proteins can be phosphorylated on serine, threonine, or tyrosine residues by protein kinases (17). Some kinases have been found to be essential for spermiogenesis and male fertility, for example, the mitogen-activated protein kinases (18), the cell cycle regulators POLO-like kinases (19), the androgen receptor p21-activated kinase 6 (20), and the testis-specific serine/threonine-protein kinase family (21) were all shown to be essential for male infertility. Previously, we systematically characterized protein phosphorylation during spermiogenesis, and the function of a kinase, homeodomain-

‡ These authors contributed equally to this work.
* For correspondence: Xuejiang Guo, guo_xuejiang@njmu.edu.cn; Jun Zhang, zhang_jun@njmu.edu.cn; Zhibin Hu, zhibin_hu@njmu.edu.cn.

interacting protein kinase 4 (HIPK4), in spermiogenesis and male infertility has been less documented (22). HIPK4 belongs to the homeodomain-interacting protein kinases family. This serine/threonine kinase is predominantly expressed in the testis (23) and has a cytoplasmic localization because it lacks a typical nuclear localization signal (24). Previous single-cell sequencing showed its expression in spermatids in human testis (25, 26). In a recent study, deletion of *Hipk4* was found to lead to male sterility with defects in the F-actin–scaffolded acroplaxome during spermatid elongation and abnormal head morphologies in mature spermatozoa (27); however, the direct substrates of HIPK4 are still not known.

Here, we examined whether *HIPK4* mutations are present in patients with NOA and identified an *HIPK4* heterozygous truncating mutation that leads to decreased protein expression. Phosphoproteomic profiling of *Hipk4* knockout (KO) testis and experimental validation further identified manchette-associated protein RIMS-binding protein 3 as a phosphorylation substrate of HIPK4. Thus, we identified HIPK4 as a novel manchette function regulator with essential roles in spermatid head shaping and male fertility.

Results

Identification of deleterious HIPK4 mutations from patients with NOA

To identify the *HIPK4*-associated mutations in human with spermatogenic defects, we conducted Sanger sequencing in coding regions of *HIPK4* from a cohort of 620 NOA patients and 2678 fertile controls (Figs. 1*A* and S1*A*). Intriguingly, 10 rare (absent in the 2678 fertile controls) and deleterious (combined annotation–dependent depletion [CADD score of >15]) variants were identified in 10 unrelated NOA-affected men (Table S2), including two heterozygous nonsense mutations (NP_653286.2: p.Lys490*, c.1468A>T and NP_653286.2: p.Arg541*, c.1621C>T) and eight heterozygous missense mutations, three of which were in the kinase catalytic domain of HIPK4 (Figs. 1*B* and S1*B*). To further evaluate the effects of these mutations *in vitro*, we overexpressed the full-length wildtype and mutant cDNA constructs in HEK293T cells. Two heterozygous nonsense mutations harboring in *HIPK4* were truncated, and the protein level of one variant (p.Lys490*, c.1468A>T) was significantly decreased compared with that of the wildtype, FLAG-tagged EGFP as transfection efficiency

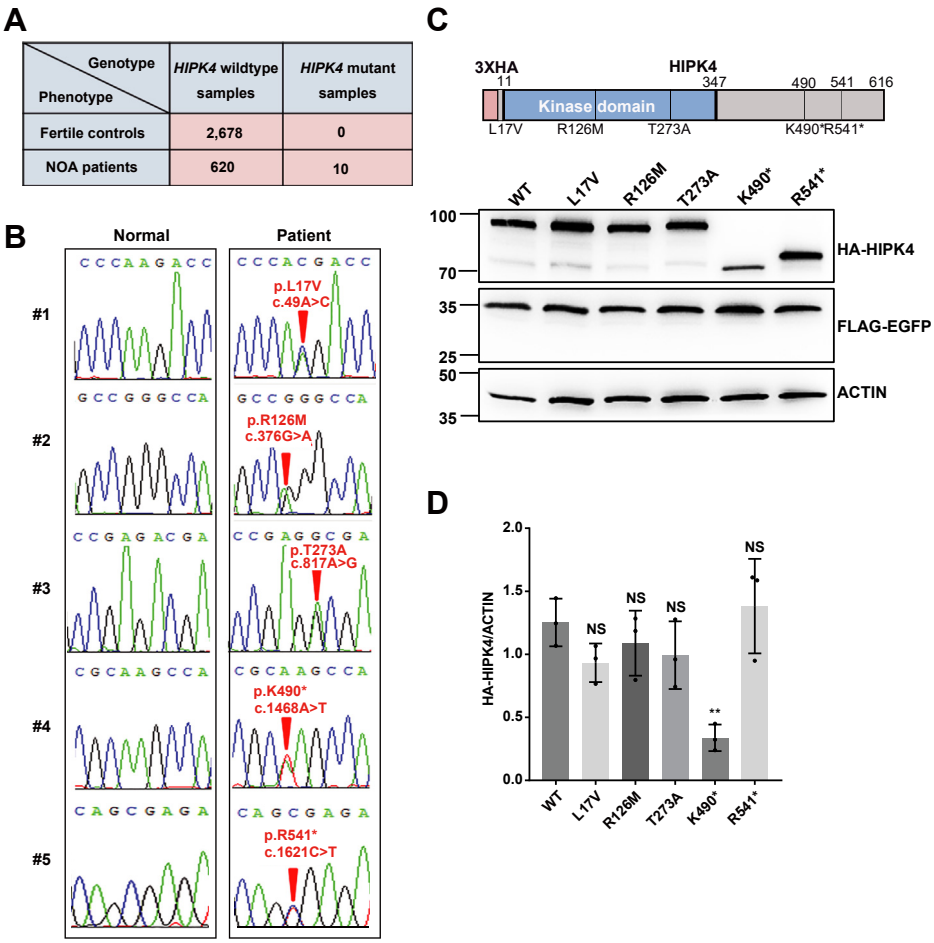

Figure 1. *HIPK4* mutations were detected in patients with NOA. *A*, the number of NOA cases and fertile controls included in the mutation analysis. *B*, sequencing graphs of five mutations identified from patients with NOA with the detected mutations annotated in *red*. *C* and *D*, western blots (*C*) and statistics analysis (*D*) of the overexpression of HA-HIPK4 with different mutations from three independent replicates, with FLAG-EGFP as a transfection control and ACTIN as a loading control. HIPK4 proteins were detected *via* the anti-HA antibody. Data are presented with the mean ± SD. $^{**}p < 0.01$ by Student's *t* test. HIPK4, homeodomain-interacting protein kinase 4; NOA, nonobstructive azoospermia.

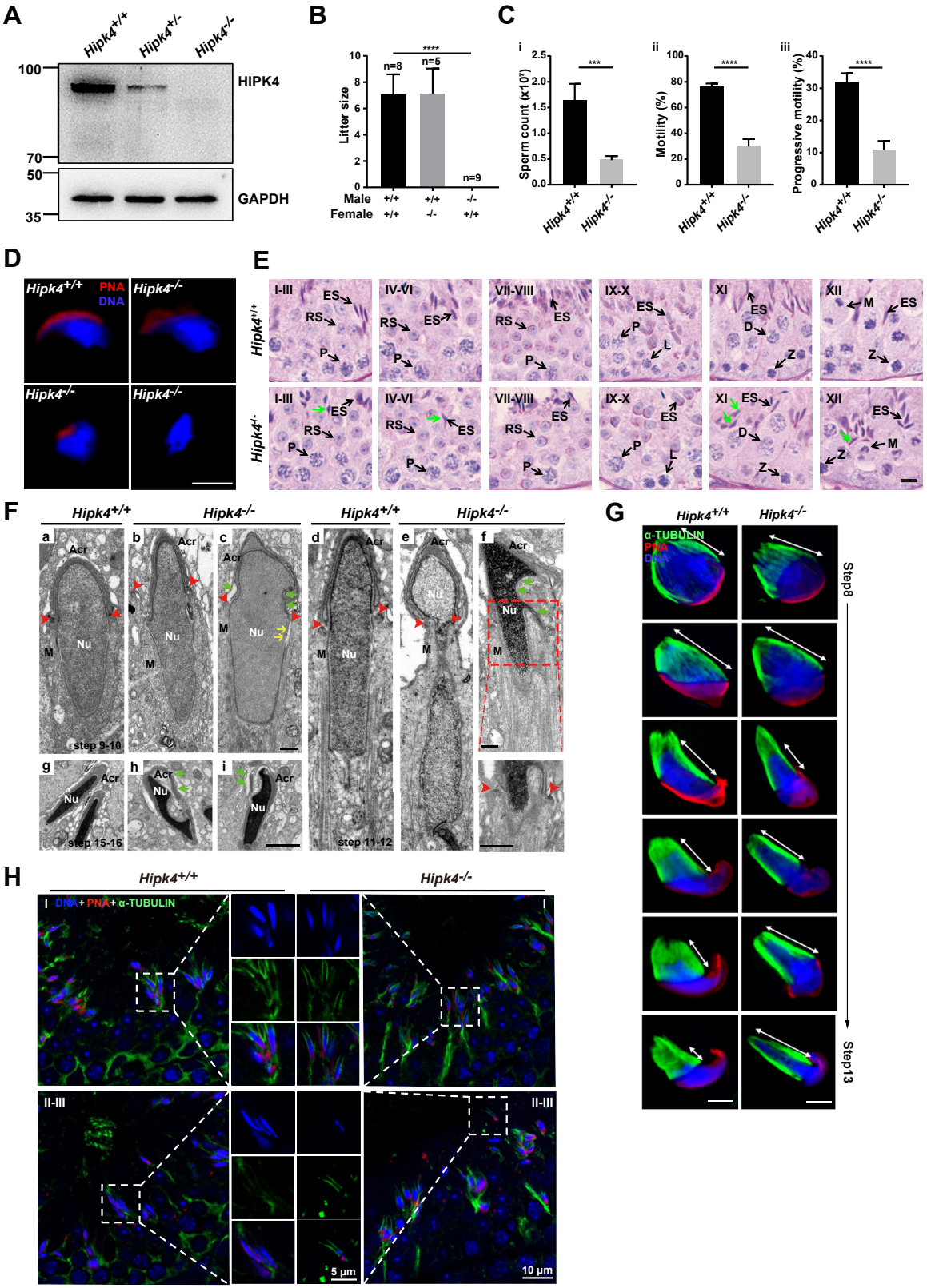

Figure 2. *Hipk4* knockout male mice are infertile with abnormal manchette. *A*, protein expression of HIPK4 in different genotypes, with GAPDH as a loading control. *B*, litter sizes of *Hipk4*$^{-/-}$ male and female mice (ANOVA with post-hoc Dunnett's *t* test). *C*, comparison of sperm count (i), sperm motility (ii), and sperm progressive motility (iii) of 8-week-old *Hipk4*$^{+/+}$ and *Hipk4*$^{-/-}$ mice (n = 3) (two-tailed Student's *t* test). *D*, immunofluorescence analysis between seminiferous tubules from *Hipk4*$^{+/+}$ and *Hipk4*$^{-/-}$ testes with acrosome stained by PNA and DNA stained by DAPI. Scale bar: 20 μm. *E*, PAS-stained different stages of seminiferous tubules from adult *Hipk4*$^{+/+}$ and *Hipk4*$^{-/-}$ testes. The *green arrow* points to abnormal nuclei of spermatids. Scale bar, 20 μm. *F*, ultrastructural analysis of *Hipk4*$^{+/+}$ and *Hipk4*$^{-/-}$ spermatids using transmission electron microscopy. *Hipk4*$^{+/+}$ elongating spermatids (steps 9–12) show normal assembly of the manchette and perinuclear ring (a and d). The perinuclear ring (*red arrow*) of elongating spermatids (steps 9–12) in *Hipk4*$^{-/-}$ is ectopically placed (detached from the nucleus) (b and f). The acroplaxome (*green arrow*) is distorted (c and f). The *yellow arrow* indicates that manchette is

control (Fig. 1, *C* and *D*). Thus, the NOA-associated mutation (NP_653286.2: p.Lys490*, c.1468A>T) could lead to decreased protein expression of HIPK4.

HIPK4 deficiency led to defective manchette formation and retained spermatids

According to previous reports, HIPK4 was largely expressed in the testis and first detected in germ cells at postnatal day 21, coinciding with the appearance of step 2 to 3 round spermatids (27), with a cytoplasmic location (24). To study *in vivo* functions of *Hipk4*, we used CRISPR/Cas9 system to generate *Hipk4* KO mice. Among the *Hipk4* mutants, female Founder #3 with a 49 bp deletion was chosen for subsequent studies (Fig. S2). Western blotting analysis detected no HIPK4 in adult *Hipk4*$^{-/-}$ mouse testis (Fig. 2*A*). *Hipk4*$^{-/-}$ females displayed normal fertility, while *Hipk4*$^{-/-}$ males were sterile (Fig. 2*B*). Compared with wildtype, dramatically decreased numbers of sperm, sperm motility, and sperm progressive motility (Fig. 2*C*, Table S3 and Movie S1) were observed.

In addition, *Hipk4*$^{-/-}$ sperm lacked a typical hook-shaped appearance and showed different degrees of acrosome defects (Fig. 2*D*). Abnormal nuclei in the elongated and condensing *Hipk4*$^{-/-}$ spermatids from steps 10 to 16 were observed (Fig. 2*E*). Similar to previous report (27), varying degrees of defects were observed using transmission electron microscope during nuclear elongation, including invaginated and/or evaginated acroplaxome containing region (Fig. 2*F*, c and f), elongated manchette along with constricted nuclear around perinuclear ring (Fig. 2*F*, e), and deviated perinuclear ring (Fig. 2*F*, b and f). At steps 15 to 16, most condensed spermatids exhibited detached acrosome, deformed nucleus, and expanded perinuclear space (Fig. 2*F*, h and i), suggesting defects in the transport along the spermatid manchette. Moreover, abnormally elongated manchette and distal movement along the nuclear surface were found in *Hipk4*$^{-/-}$ elongating spermatids (Figs. 2*G* and S3*A*) and persistent in steps 13 to 14, whereas the manchette had already disappeared in wildtype (Fig. 2*H*).

The increased unreleased spermatids with delayed spermiation in stage IX of *Hipk4*$^{-/-}$ mice (Fig. 3, *A* and *B*) caused us to focus on apical ectoplasmic specialization (ES). ES is a kind of adhesion junction based on microfilaments (F-actin) (28–30), and retained apical ES between spermatids and Sertoli cells in stage IX has been shown to lead to delayed spermiation (11). Staining of ESPIN, a marker for ES, showed retained spermatids in stage IX–X without ES structures in *Hipk4*$^{-/-}$ mice (Figs. 3*C* and S3*B*), suggesting the spermatids had completed the earlier phases of spermiation but failed disengagement. Therefore, a significant proportion of spermatids were not released from Sertoli cell and instead phagocytosed, resulting in fewer sperm entering the epididymis. As expected, TUNEL staining revealed increased numbers of apoptotic cells in *Hipk4*$^{-/-}$ seminiferous tubules, which were predominantly present in stage IX to X (Figs. 3, *D* and *E* and S3*C*). TUNEL staining and cyclical variations of the apoptotic cells strongly supported an origin from phagocytized spermatids.

Phosphoproteomic analysis of Hipk4$^{-/-}$ *testes revealed downstream phosphorylation substrates*

To explore the mechanisms by which HIPK4 functions during spermiogenesis, we used multiplexed tandem mass tags (TMT) labeling and a tandem mass spectrometry (LC-MS/MS) approach to quantify the proteome and phosphoproteome of testes from *Hipk4*$^{-/-}$ and *Hipk4*$^{+/+}$ mice. Altogether, 10,621 proteins were quantified, and only 47 proteins showed differential expression levels after *Hipk4* KO, comprising six upregulated proteins and 41 downregulated proteins (Fold change > 1.5 and $p < 0.05$) (Fig. S4, *A* and *B* and Table S4). Gene ontology (GO) analysis of the 47 differentially abundant proteins showed no enrichment of any terms in biological process or cellular localization. Phosphoproteomic profiling identified 31,331 phosphorylation sites, corresponding to 6142 phosphorylated proteins, with 513 differential phosphorylation sites corresponding to 359 proteins between the *Hipk4*$^{-/-}$ and *Hipk4*$^{+/+}$ groups after normalization against the protein expression levels (localization probability > 0.75, multiplicity = 1, fold change > 1.5 and $p < 0.05$). The number of differentially phosphorylated proteins induced by *Hipk4* KO was significantly higher than that of differentially abundant proteins, suggesting that HIPK4 mainly affected the phosphorylation of proteins. Among the differential phosphorylation sites, 475 sites corresponding to 332 phosphoproteins were downregulated, but only 38 sites were upregulated (Fig. 4, *A* and *B* and Table S4), consistent with the loss of kinase function after *Hipk4* KO. The proteins with downregulated phospho-sites can be potential phosphorylation substrates of the HIPK4 kinase. GO analysis of these 332 downregulated phosphoproteins showed significant enrichment in "microtubule" (20/332), "microtubule organizing center part (18/332)", "motile cilium" (16/332), "acrosomal vesicle" (10/332), "sperm flagellum" (8/332), "microtubule associated complex" (8/332), and "sperm principal piece" (3/332) (Fig. 4*C* and Table S5). Besides, "microtubule-based movement" in cellular component terms (16/332), "nucleocytoplasmic transport" (14/332),

not attached to the nucleus (c). The manchette is elongated and the perinuclear ring shows abnormal constriction in spermatids (e). The mutant condensed spermatids frequently contain deformed nuclei and detached acrosomes (*green arrow*), with an expanded perinuclear space (h and i). Scale bars: 1 μm. *Arrow* (*red*), perinuclear ring. Box is high amplification. *G*, spermatids isolated from *Hipk4*$^{+/+}$ and *Hipk4*$^{-/-}$ mice were stained for α-TUBULIN (*green*) at different manchette-containing steps. The distance between the perinuclear ring and the caudal side of the head is indicated by *double-headed arrows*. Scale bar: 5 μm. *H*, manchette clearance is delayed in *Hipk4*$^{-/-}$ mice. During stages II–III the manchette has disappeared in the *Hipk4*$^{+/+}$ mouse but was retained in the *Hipk4*$^{-/-}$ mouse. α-TUBULIN (*green*) was used to visualize manchette microtubules, with DNA stained by DAPI (*blue*), and acrosome stained by PNA (*red*). Data are presented with the mean ± SD. ***$p < 0.001$; ****$p < 0.0001$. D, diplotene; ES, elongated spermatids; HIPK4, homeodomain-interacting protein kinase 4; L, leptotene; M, metaphase; Nu, nucleus; P, pachytene; RS, round spermatids; Acr, acrosome; M, manchette; Z, zygotene.

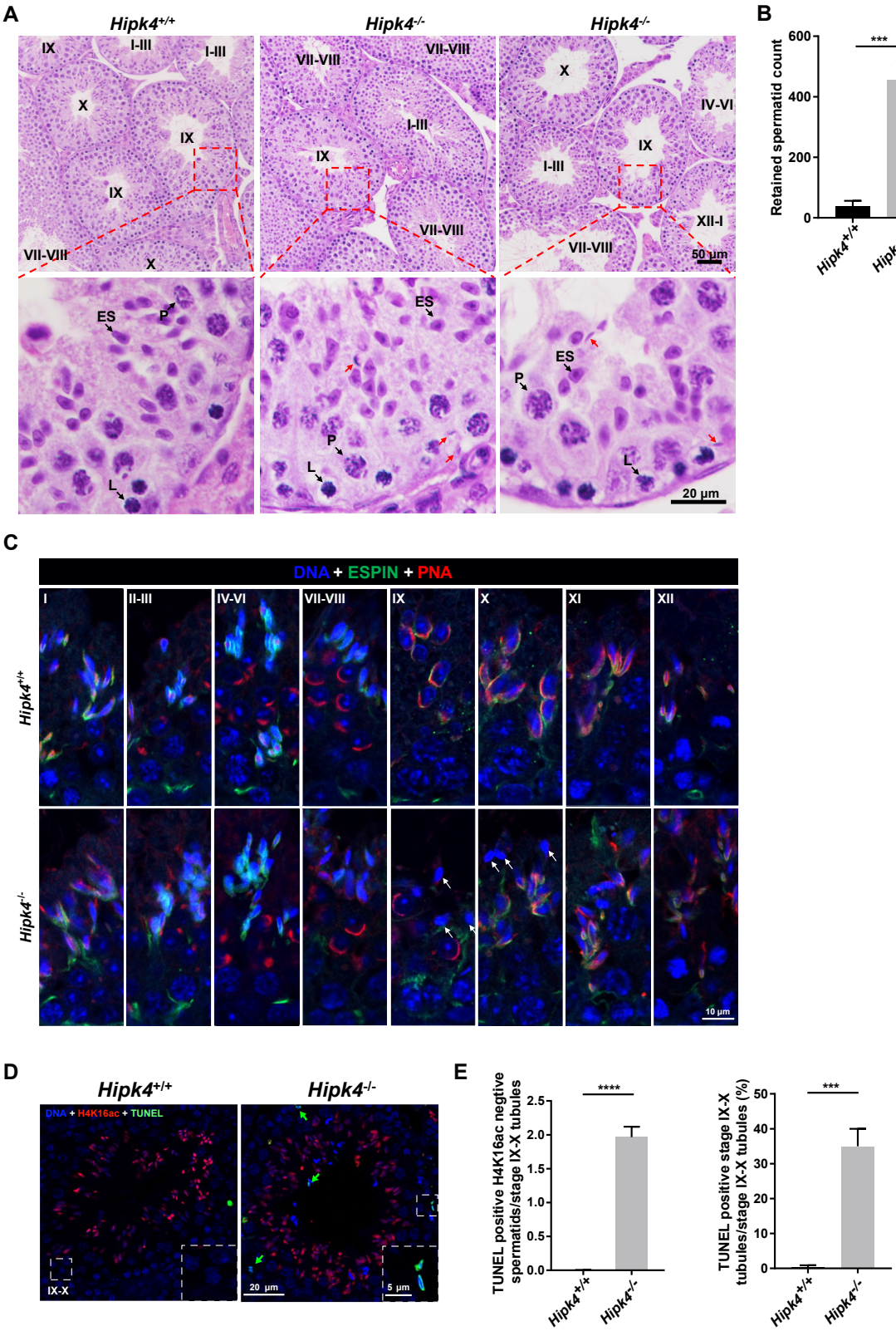

Figure 3. *Hipk4* knockout testes show retained spermatids. *A*, cross sections of *Hipk4*$^{+/+}$ and *Hipk4*$^{-/-}$ mouse testes with stages of seminiferous tubules labeled, scale bar, 50 μm. Retained spermatids in stage IX tubules are shown in *red arrow*. scale bar, 20 μm. *B*, statistics analysis of retained spermatids from 25 tubules in three replicates (Student's *t* test). *C*, Immunofluorescence of seminiferous tubules from control and *Hipk4*$^{-/-}$ testes using mouse anti-ESPIN antibody with acrosome stained by PNA and DNA stained by DAPI. The *arrows* indicate unreleased spermatids. Scale bars: 10 μm. *D*, TUNEL in stage IX–X *Hipk4*$^{+/+}$ and *Hipk4*$^{-/-}$ seminiferous tubules (30 round tubules analyzed for each genotype). TUNEL (*green*), DNA (*blue*), and H4K16ac (*red*), a marker for elongating spermatids. *Arrows* (*green*) indicate TUNEL-positive spermatids. Scale bar, 20 μm. Box is high amplification. *E*, quantitative analysis of TUNEL staining in stage IX–X *Hipk4*$^{+/+}$ and *Hipk4*$^{-/-}$ seminiferous tubules (Student's *t* test, 30 round tubules analyzed for each genotype). Data are presented as the mean ± SD. ***$p < 0.001$; ****$p < 0.0001$. ES, elongated spermatid; L, leptotene; P, pachytene

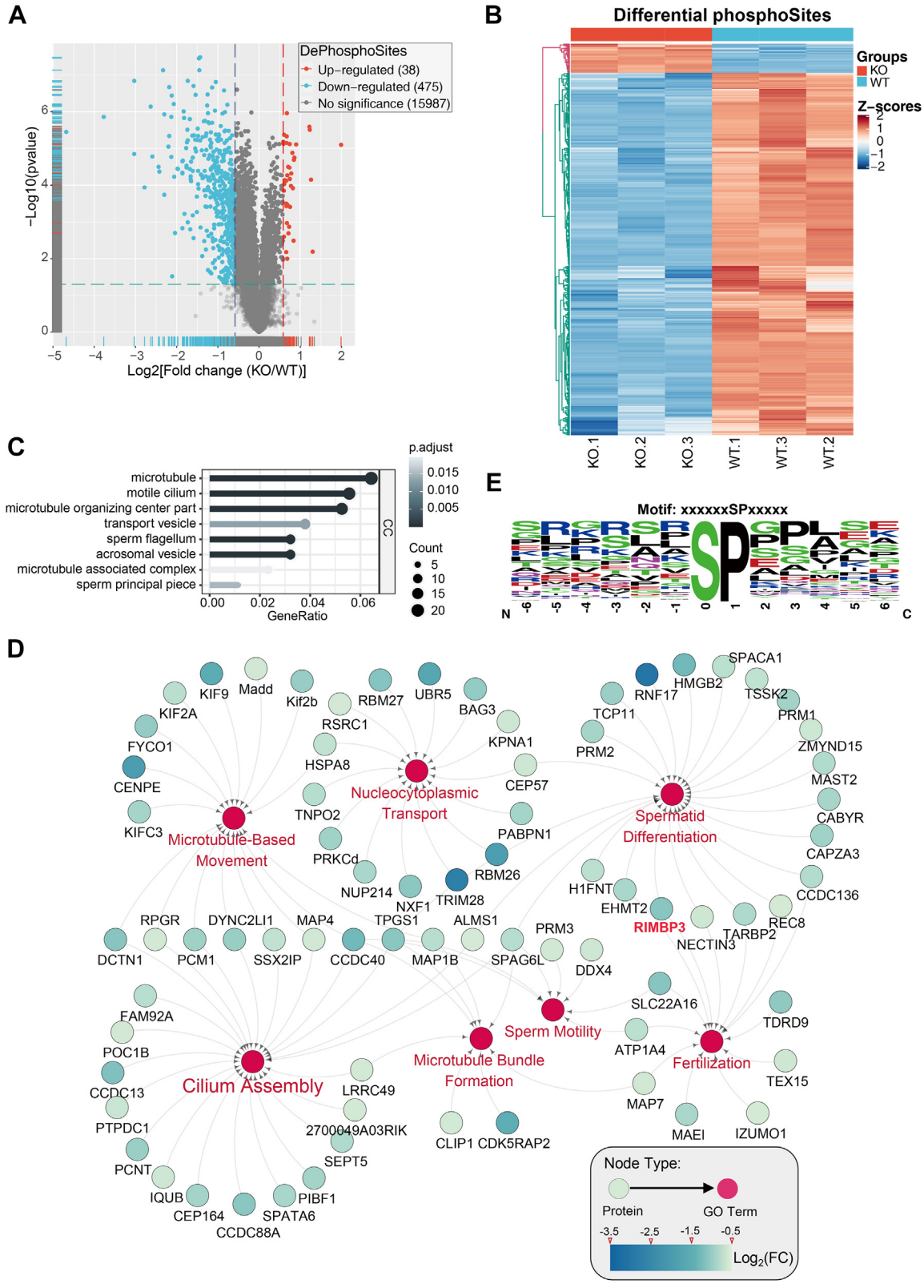

Figure 4. Phosphoproteomic profiling of *Hipk4* knockout testicular proteins. *A*, the volcano plot of quantified protein phosphorylation sites between *Hipk4*$^{+/+}$ and *Hipk4*$^{-/-}$ mice. The cutoff values (localization probability > 0.75, multiplicity = 1, fold change >1.5, and $p < 0.05$) were utilized to identify phosphorylation sites with significantly differential levels. *B*, heatmap of differentially regulated phosphorylation sites. The Euclidean distance metric and the complete linkage clustering algorithm were used. *C* and *D*, Gene ontology annotations of the downregulated phosphorylated proteins in *Hipk4*$^{-/-}$ mice testes. Enriched terms of cellular components (*C*) and biological processes (*D*) are shown as a bar graph and a network by Cytoscape, respectively. *E*, the most enriched motif among 475 downregulated phosphorylation sites in *Hipk4*$^{-/-}$ testes was identified using the Motif-X algorithm. The height of the residues represents the frequency with which they appear at the respective positions. The color of the residues represents their physicochemical properties.

"spermatid differentiation" (22/332), "microtubule bundle formation" (8/332), "sperm motility" (7/332), "fertilization" (13/332), and "cilium assembly" (23/332) were the enriched biological process terms (Fig. 4*D* and Table S5). The analysis demonstrated regulatory roles of HIPK4 in spermiogenesis and sperm functions through phosphorylation. Kinase specificity is defined by the amino acid sequences surrounding the phosphorylation sites (31); therefore, we employed the Motif-X algorithm (32) using a sequence window of ±six amino acids around the identified phosphorylated site to predict consensus phosphorylation site motifs. The most significantly enriched motif was xSPx (p = 9.50E-12) (amino acids with low probability in modification site motif visualization were replaced with letter "x" in phospho-peptides); the corresponding conserved sequence logos were generated by WebLogo (33) (Fig. 4*E*). Interestingly, this most enriched motif, xSPx, is also recognized by HIPK2, another member of HIPK family (34, 35), which suggested that the kinase specificity might be conserved among the HIPKs.

Manchette-associated protein RIMBP3 is a phosphorylation substrate of HIPK4

The quantitative phosphoproteomic profiling identified four phosphorylation sites (Ser15, Ser21, Ser263, and Ser347) as xSPx motif in RIMBP3, which were all significantly downregulated after *Hipk4* KO and located in the N-terminal region of RIMBP3 (Fig. 5, *A* and *B*). RIMBP3 is a manchette-associated protein, previously reported to be essential for manchette formation, playing a key role in sperm head morphogenesis during the late stages of sperm development (16). *Rimbp3* deletion phenocopied the malformed nucleus of *Hipk4*$^{-/-}$ spermatids (16), which suggested that RIMBP3 might be a potential HIPK4 phosphorylation substrate. To validate whether the N terminus of RIMBP3 is phosphorylated by HIPK4, we performed Phos-tag Western blotting, which allows the detection of phosphorylation by reducing the electrophoretic mobility of phosphorylated protein using Phos-tag, a phosphorylated amino acid chelator. When *Rimbp3* encoding an N-terminally truncated (1–460 AA) protein was cotransfected with *Hipk4* into HEK293T cells, phosphorylated RIMBP3 and autophosphorylated HIPK4 showed altered migration behavior using Phos-tag, but no change in migration of RIMBP3 and HIPK4 occurred when using kinase-dead mutant HIPK4 (Y175F) (24) (Fig. 5*C*). To detect the potential interaction between RIMBP3 and HIPK4, we overexpressed HA-tagged HIPK4 with FLAG-tagged full-length RIMBP3 in HEK293T cells, and co-immunoprecipitation (IP) analysis indicated that RIMBP3 interacted with HIPK4 in HEK293 cells (Fig. 5*D*). Furthermore, we immunoprecipitated RIMBP3 from testis lysates using anti-RIMBP3 antibodies, which also identified HIPK4 as an interacting protein of RIMBP3 in testis (Fig. 5*E*). Thus, RIMBP3 is a phosphorylation substrate of HIPK4. HIPK4 was reported to be expressed in steps 3 to 8 spermatids (27), while RIMBP3 was expressed in the cytoplasm of spermatocytes and round spermatids and was mainly located in the manchette of elongating spermatids (16) (Figs. 6*A* and S3*D*). RIMBP3 plays a critical role in manchette organization and function; therefore, we wanted to know whether RIMBP3 localization and the manchette were affected in *Hipk4* null mice. Immunofluorescence analysis showed that RIMBP3 and α-TUBULIN were co-localized in the manchette (Fig. 6*B*). After *Hipk4* KO, RIMBP3 and α-TUBULIN co-localized manchette showed abnormal shape in spermatids of steps 11 to 12. Collectively, these results suggested that HIPK4 regulates manchette formation and function at least partly through phosphorylation of RIMBP3, thus playing an essential role in sperm head shaping (Fig. 6*C*).

Discussion

HIPK4 is a serine/threonine kinase that is predominantly expressed in mouse testis. Despite *Hipk4*-defective mice displaying male infertility, the exact roles of HIPK4 in spermatogenesis remain unclear. In this study, we identified ten heterogeneous mutations in *HIPK4* from patients with NOA and demonstrated that nonsense mutant (p. Lys490*, c.1468A>T) decreased protein expression. The *Hipk4* KO mice showed male infertility with defects in spermiogenesis which led to malformed sperm heads, which was consistent with Crapster *et al.*'s findings (27). In *Hipk4*$^{-/-}$ mice, phosphoproteomic profiling mainly showed downregulated phosphorylation, suggesting essential roles of HIPK4 in spermiogenesis. Moreover, we also demonstrated that a manchette-associated protein, RIMBP3, was a substrate of HIPK4. Overall, our study showed that HIPK4 is associated with human spermatogenesis, which is an important regulator of manchette formation and function, and essential for sperm head shaping.

Previous studies have shown that a proportion of idiopathic human male infertility, often accompanied by azoospermia or severe oligospermia, is caused by genetic defects (36, 37). In this study, we found that the *Hipk4* KO mice presented OAT, while we detected deleterious *HIPK4* mutations in patients with NOA, which is a more severe form of spermatogenesis abnormality. Actually, human azoospermia does not mean that the testis cannot produce sperm. Although no sperm could be observed in semen, studies show that sperm could be retrieved surgically from 43 to 63% of patients with NOA and could be used for assisted reproduction (38). Idiopathic NOA is a complex, highly polygenic, and environmentally affected disease (39). Environmental factors can cause spermatogenesis abnormalities (40, 41) and might interact with genetic mutations, leading to more severe phenotypes in humans. Common mutations in the human genome, mainly single nucleotide polymorphisms and copy number variations, might also play roles in spermatogenesis failure (42) and might interact with the mutations of *HIPK4*. However, the mice used in this study were inbred with a pure genetic background. Different phenotypes between mice and humans have been reported for many other genes. For example, mutations of *DNAH1* can lead to multiple morphological abnormalities of the sperm flagella and male sterility in humans (43); however, invalidation of the mouse ortholog, *Mdhc7*, caused male sterility with the

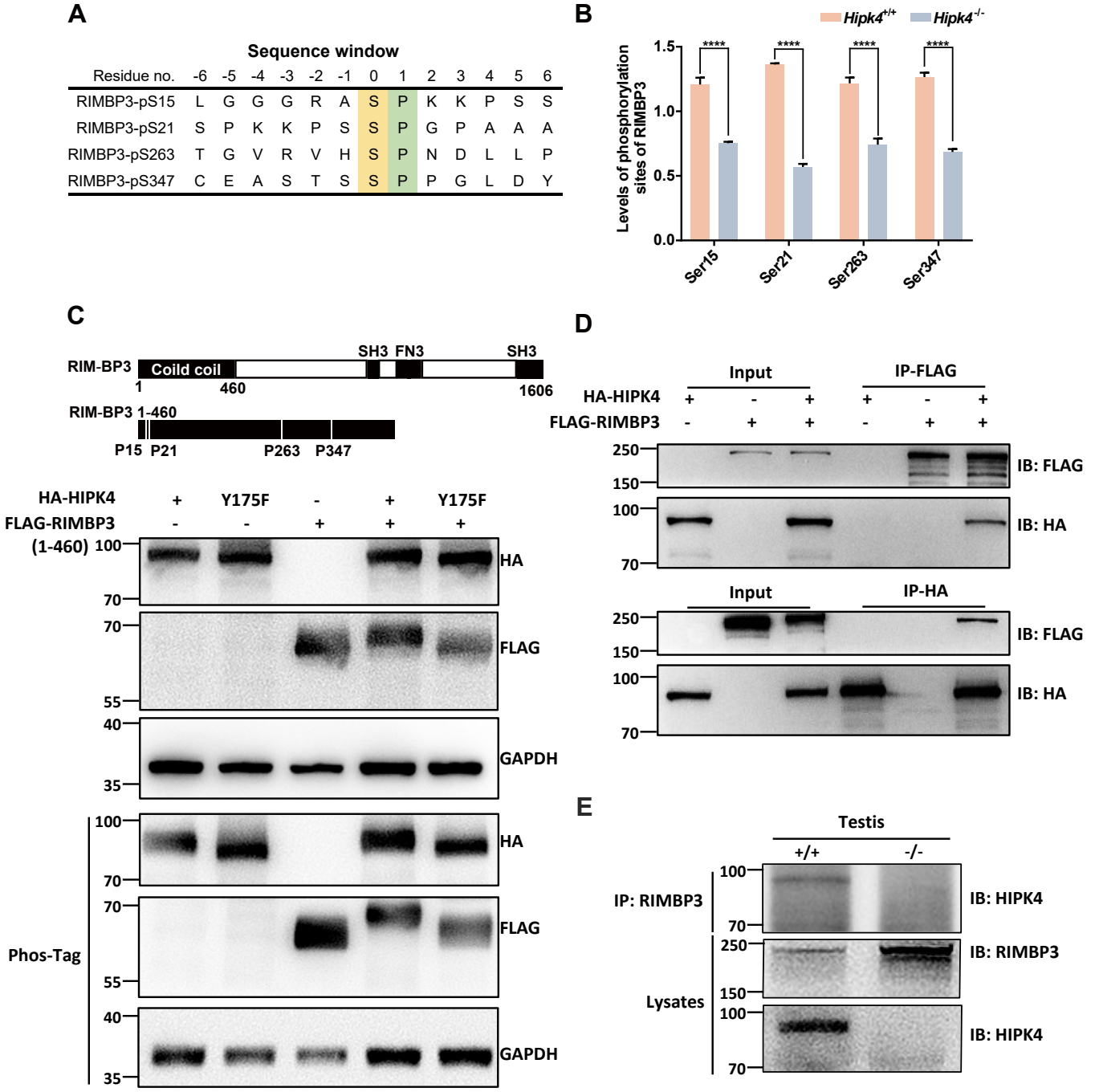

Figure 5. RIMBP3 is a phosphorylation substrate of HIPK4. *A*, four downregulated phosphor-peptides from RIMBP3 present an xSPx motif. *B*, the level of different phosphorylation sites in RIMBP3 from the quantitative phosphoproteomics data. Data are shown as the mean ± SD (n = 3), ****$p < 0.0001$. *C*, Western blotting analysis of overexpressed HA-HIPK4 or HA-HIPK4 (Y175F) in HEK293T cell together, with or without FLAG-RIMBP3 (1–460) using a Phos-tag gel with GAPDH as a loading control. *D*, interaction between HA-HIPK4 and FLAG-RIMBP3 *in vitro* validated in HEK293T cell. *E*, interaction between HIPK4 and RIMBP3 *in vivo* in mouse testis. HIPK4, homeodomain-interacting protein kinase 4; RIMBP3, RIMS-binding protein 3.

decreased motility, but no morphological defects of the sperm tail were observed (44). Therefore, it is reasonable to see *HIPK4* mutations in NOA and OAT in *Hipk4* KO mice.

A previous study revealed F-actin scaffolded acroplaxome defects in elongating spermatids and abnormal sperm head morphologies in *Hipk4*-null mice (27), but the distinct substrates and regulatory mechanisms of HIPK4 in spermiogenesis are still unknown. Similar to that, we also found a comprehensive abnormality of the acrosome–acroplaxome–manchette complex after *Hipk4* KO, including a distorted acroplaxome, a detached acrosome, elongated and symmetric conical manchette, and the ectopic positioning of the perinuclear ring. The acrosome–acroplaxome–manchette complex was thought to define the specific shape of the sperm head (45). The acroplaxome is tightly bound to the acrosome. It shapes the apical portion of the spermatid head and might provide a scaffold to regulate exogenous constriction forces produced by Sertoli cell F-actin hoops (46). The manchette

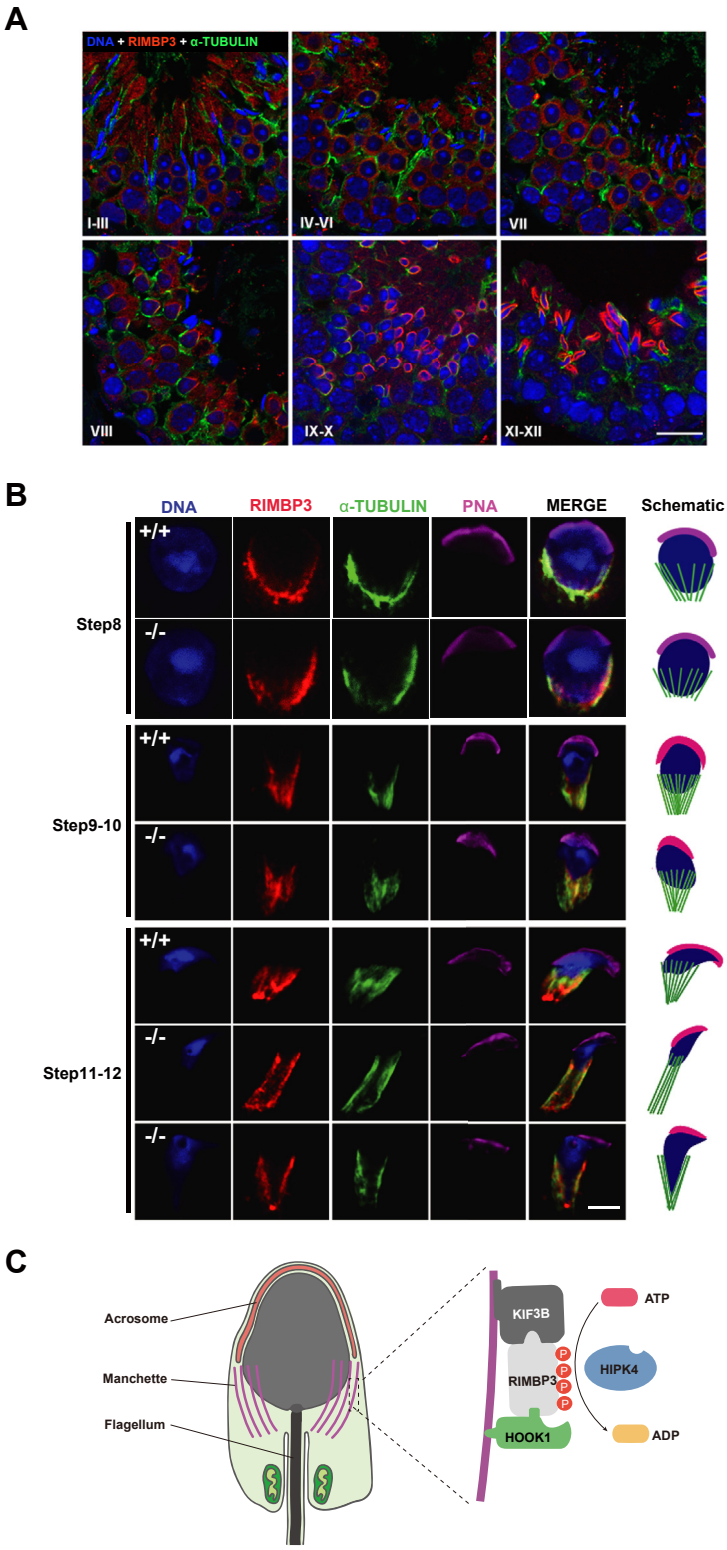

Figure 6. HIPK4 regulates sperm head shaping *via* phosphorylating RIMBP3. *A*, localization of RIMBP3 in seminiferous tubules from *Hipk4*$^{+/+}$ mice. RIMBP3 was mainly located in the manchette of elongating spermatids and also expressed in spermatocytes and round spermatids. IF staining of RIMBP3 (*red*) and α-TUBULIN (*green*) in seminiferous tubules from *Hipk4*$^{+/+}$ mice with nuclei stained by DAPI. Scale bar, 10 μm. *B*, the localization of RIMBP3 in the manchette of steps 11 to 12 spermatids were affected after deletion of *Hipk4*. Co-immunofluorescence of RIMBP3 together with manchette stained by anti-α-TUBULIN, acrosome stained by PNA, and DNA stained by DAPI in *Hipk4*$^{+/+}$ and *Hipk4*$^{-/-}$ spermatids from step 8 to step 11 to 12 during spermiogenesis. Schematic diagrams of *Hipk4*$^{+/+}$ and *Hipk4*$^{-/-}$ spermatids at different steps showing shape of the nucleus (*blue*), acrosome (*purple*), and manchette (*green*) are on the right. Scale bar: 5 μm. *C*, a theoretical model shows that HIPK4 phosphorylates RIMBP3 and regulates manchette during spermatogenesis. HIPK4, homeodomain-interacting protein kinase 4; RIMBP3, RIMS-binding protein 3.

shapes the basal portion of the spermatid head and moves distally in conjunction with the constriction of the perinuclear ring (46). Further mechanistic studies revealed a substrate of HIPK4, the adaptor molecule RIMBP3, deletion of which showed similar acrosome–acroplaxome–manchette complex abnormalities (16). Previous studies also showed that RIMBP3 regulates the development and function of manchette by interacting with hook microtubule tethering protein 1 (HOOK1) and kinesin family member 3B (16). HOOK1 also is a manchette-associated protein, whose mutation caused abnormal sperm heads (47). Kinesin family member 3B is microtubule-based molecular motor protein responsible for intramanchette transport (48). Thus, HIPK4 might regulate spermatid head morphogenesis by regulating the acrosome–acroplaxome–manchette complex through RIMBP3. Besides, *Kif3a*, *Cep131*, *Lrguk1*, and *Spef2* mutant mice (14) showed that the manchette also plays an important role in flagellum formation; however, the ultrastructure of *Hipk4*$^{-/-}$ sperm flagellum is normal and similar to that of *Rimbp3* and *Hook1* defective mice. It seems that abnormalities of certain manchette proteins may not necessarily lead to a disorder of the flagellum structure. HIPK4 mainly regulates RIMBP3, a manchette protein essential for sperm head but not flagella formation.

Previous studies have shown that the C terminus of RIMBP3 interacts with HOOK1 to regulate the development of the manchette (16); however, the function of its N terminus is unknown. Protein phosphorylation can change its overall structure and regulate its functions (49). Here, we found that HIPK4 could phosphorylate the N terminus of RIMBP3. HIPK4 and RIMBP3 were both expressed in steps 3 to 8 of spermatid development, and RIMBP3 continued to be expressed until step 13 (16). From step 8, RIMBP3 was highly expressed in the manchette of elongating spermatids. Phosphorylation of RIMBP3 might be regulated in an early step by HIPK4, with its functions regulated in subsequent stages. Our phosphoproteomic analysis showed a decreased phosphorylation level of HIPK4 in the *Hipk4* KO testis. Therefore, we speculated that phosphorylation of RIMBP3 by HIPK4 plays important roles in the functions of the manchette during spermiogenesis.

In summary, our work demonstrates that phosphorylation is essential for spermatogenesis, and decreased phosphorylation of microtubule-associated proteins might affect microtubule structure and function within this process. Furthermore, as a kinase predominantly expressed in spermatids, HIPK4 might serve as a potential target for male contraception.

Experimental procedures

All primer sequences and antibodies are given in Table S1.

NOA patients' information

Approval was granted by research ethics committee of Nanjing Medical University before sample collection. Studies in this work abide by the Declaration of Helsinki principles. Six hundred and twenty NOA patients and 2678 male controls with informed consent were recruited from Clinical Center of Reproductive Medicine in Nanjing. All infertile male subjects were genetically unrelated Han Chinese and screened based on andrological examinations, including a detailed medical history, physical examination, semen analysis, scrotal ultrasound, hormone assessment, karyotyping, and Y chromosome microdeletion screening. Those with a history of cryptorchidism, vascular trauma, orchitis, obstruction of the vas deferens, abnormalities in chromosome number, or microdeletions of the azoospermia factor region on the Y chromosome were excluded. Semen analysis for sperm concentration, motility, and morphology was performed according to the guidelines of World Health Organization (WHO) (2010) (50). NOA patients lack detectable sperm in their ejaculate; therefore, to differentiate NOA from obstructive azoospermia, only those with idiopathic azoospermia with small and soft testis, normal fructose and neutral alpha glucosidase in seminal plasma were included, and vasectomized patients were excluded. For a reliable diagnosis, each subject was examined twice, only those with an absence of spermatozoa from both replicates were taken to indicate azoospermia. While each control subject had fathered one healthy child or more. A 5-ml whole blood sample was obtained from each participant as a source of genomic DNA for further Sanger sequencing analysis.

Mice and cell line

Approval was granted by Animal Ethical and Welfare Committee of Nanjing Medical University before animal studies. To generate *Hipk4* KO mice, paired single guide RNAs (sgRNAs, Fig. S2*B*) were designed to target exon 3 of *Hipk4*. The oligonucleotides used to generate the sgRNA expression plasmid were annealed and cloned into the pGL3-U6-sgRNA-PGK-puromycin (Addgene plasmid # 51133). Transcription and microinjection of CRISPR/Cas9 were performed *in vitro* as described previously (51). Briefly, the Cas9 plasmid (pST1374-NLS-flag-linker-Cas9, Addgene plasmid # 44758) was linearized using AgeI and transcribed using a T7 Ultra Kit (Ambion), pGL3-T7-sgRNA-PGK-puromycin expression vectors were linearized by BsaI and transcribed using the MEGAshortscript Kit *in vitro* (Ambion). A mixture of Cas9 mRNA and two sgRNAs were injected into the cytoplasm and male pronucleus of the zygote *via* electroporation. Embryos were implanted into pseudo-pregnant C57BL/6J females according to standard procedures. Founder mice were backcrossed to C57BL/6J. All animal experiments in this study were approved by the Institutional Animal Care and Use Committee of Nanjing Medical University, Nanjing, China. All mice were housed in a specific pathogen-free animal facility under standard conditions.

The cell line HEK-293T (*Homo sapiens*) cells were used by experiments for this paper.

Point mutation plasmid construction

In vitro point mutation plasmid construction used a ClonExpress II One Step Cloning Kit (Vazyme, C112-02), with specific primers according to the manufacturer's instructions.

Histological analysis

For hematoxylin and eosin staining, the epididymis was fixed with modified Davidson fluid (30% of a 37–40% formaldehyde stock solution, 15% ethanol, 5% glacial acetic acid, and 50% distilled water) and embedded in paraffin. Sections were cut at 5-μm thickness. The sections were dewaxed with xylene, hydrated, stained, dehydrated with ethanol (70%, 80%, 90%, 100%), and blocked with resin. For PAS staining, the sections were deparaffinized, hydrated, stained with PAS reagent, counterstained with hematoxylin, dehydrated, and blocked.

Electron microscopy

Samples were fixed at 4 °C overnight with 2.5% glutaraldehyde in 0.2 M cacodylate buffer, washed with 0.2 M cacodylate buffer, dehydrated in a graded series of ethanol, embedded, and polymerized using an automated microwave tissue processor (Leica EM AMW). After polymerization, the samples were cut into 1 mm^3 pieces using a LEICA Ultracut UCT ultramicrotome. Ultrathin sections were stained with uranyl acetate and lead citrate and then examined by transmission electron microscope (JEOL, JEM-1010).

Immunofluorescence and TUNEL assay

For immunofluorescence, the sections were subjected to heat-induced antigen retrieval with citrate buffer (1.8 mM citric acid, 8.2 mM sodium citrate, pH 6.0) and washed with phosphate-buffered saline (PBS), immersed in 0.1% PBS-Triton X-100, blocked with 5% donkey serum, and incubated with primary antibodies overnight at 4 °C. After incubated with secondary antibodies and Hoechst 33258, the samples were sealed with 50% glycerol. The TUNEL staining assay kit (Vazyme) was used for apoptosis detection according to the manufacturer's instructions.

Western blotting

Cells or tissues were homogenized in cold radioimmunoprecipitation assay buffer containing protease inhibitor cocktail (Bimake, B14002). While for sperm samples, the sperm were rinsed with PBS and treated with hypotonic lysate (0.1% SDS, 0.5% Triton X-100) and resuspended with lysis buffer (250 mM Tris-HCl pH 8.8, 50 mM EDTA, 500 mM dithiothreitol, 10% SDS, 50% glycerol). Lysate was centrifuged at 10,000*g* at 4 °C for 1 h. The supernatant was collected, and the protein concentration was determined using bicinchoninic acid assay.

Equivalent amounts of proteins were separated using SDS-PAGE, transferred onto nitrocellulose membrane, blocked using 5% skim milk, and incubated with primary antibodies overnight at 4 °C. Secondary antibodies conjugated with were used to visualize specific protein bands.

The phos-tag gels contained 20 μM Phos-tag (APExBIO, F4002) and 40 μM $MnCl_2$. Before transferring onto nitrocellulose Membrane, phos-tag gel was immersed in transmembrane buffer containing 10 mM EDTA and washed to eliminate manganese ions.

Sperm analysis

Sperm from the epididymal tail were incubated in HTF medium (Irvine Scientific) supplemented with 10% fetal bovine serum at 37 °C for 5 min. Sperm motility assessments were performed using the Hamilton Thorne's Ceros II system (Hamilton-Thorne Research).

Protein sample preparation, digestion, and TMT labeling

Testes from three mice from each of the KO and control groups were subjected to protein extraction, digestion, and TMT labeling. In brief, testicular tissues were lysed with protein extraction buffer (8 M urea, 75 mM NaCl, 50 mM Tris, pH 8.2, 1% (vol/vol) EDTA-free protease inhibitor, 1 mM NaF, 1 mM β-glycerophosphate, 1 mM sodium orthovanadate, 10 mM sodium pyrophosphate) (Sigma-Aldrich) followed by sonication and centrifugation, with protein concentrations determined by the Bradford assay (Beyotime). Cysteine residues were reduced using 5 mM dithiothreitol (Thermo Fisher Scientific) and alkylated using 14 mM iodoacetamide (Sigma-Aldrich). Proteins were digested overnight at 37 °C with 5 ng/μl trypsin (Promega) with 1 mM $CaCl_2$ (Sigma-Aldrich). The peptides were subjected to TMT 6-Plex (Thermo Fisher Scientific) labeling, mixed, and desalted using a Waters tC18 Sep-Pak column (Waters).

LC-MS/MS measurements and data processing

The TMT-labeled peptide mixture was fractionated using an ACQUITY UPLC M-Class with XBridge BEH C18 column (300 μm × 150 mm, 1.7 μm; 130 Å, Waters) with 30 fractions collected by nonadjacent pooling scheme using a 128-min gradient of 3% buffer B (A: 10 mM ammonium formate, pH 10; B: 100% acetonitrile) for 14 min, 3% to 8% B for 1 min, 8% to 29% B for 71 min, 29% to 41% B for 12 min, 41% to 100% B for 1 min, 100% B for 8 min, 100% to 3% B for 1 min, followed by 20 min at 3% B.

For phosphoproteomic quantification, the TMT-labeled peptide mixture was fractionated using Agilent 1260 system with XBridge BEH300 C18 column (10 × 250 mm, 5 μm; Waters) into ten fractions using a nonadjacent pooling scheme. TMT-labeled phospho-peptides were enriched through $Ti4^+$-IMAC (immobilized metal affinity chromatography, J&K Scientific). In short, peptides from each fraction were dissolved in loading buffer (80% acetonitrile, 6% trifluoroacetic acid (TFA)) and incubated with IMAC beads for 30 min, washed with wash buffer I (50% acetonitrile, 200 mM NaCl, 6% TFA) and II (30% acetonitrile, 0.1% TFA) for 30 min, respectively, and eluted using elution buffer (10% NH_4OH) for 15 min. The eluates of phospho-peptides were dried and desalted using C18 StageTips (Thermo Fisher Scientific).

For LC-MS/MS analyses, TMT-labeled peptides or enriched TMT-labeled phospho-peptides were resuspended in 0.1% FA

and analyzed using an Orbitrap Fusion Lumos Tribird mass spectrometer (Thermo Fisher Scientific) coupled to the Easy-nLC 1200 high performance liquid chromatography, using a 95 min linear gradient (3%–5% buffer B for 5 s, 5%–15% buffer B for 40 min, 15%–28% buffer B for 34.8 min, 28%–38% buffer B for 12 min, 30% buffer to 100% buffer B for 5s and to 100% buffer B for 8 min) (buffer A: 0.1% FA; buffer B: 80% acetonitrile, 0.1% FA). The Orbitrap Fusion Lumos Tribrid Mass Spectrometer was operated in the data-dependent mode. A full survey scan was obtained for the m/z range of 350 to 1500. For both protein expression and phosphorylation quantification, the resolution of HCD MS/MS was 15,000.

Bioinformatics analysis

Raw files were searched against the mouse protein sequences obtained from the Universal Protein Resource (UniProt, 2018/07/18) database with MaxQuant software (version 1.6.5.0) (52) under default parameters, except that the optional modification of phosphorylation (S/T/Y) was used for phosphorylation data. The expression level of each phosphorylated site was normalized against the abundances of the corresponding protein. Only type I phosphorylation sites with a localization probability >0.75 were used for the downstream analysis. To obtain an overview of the function of proteins identified by our proteomic analyses, GO enrichment analysis was performed using "clusterProfiler" package (53) in R. The network of biological process was constructed using Cytoscape (version 3.7.1) (54). *p*-values were adjusted considering the false discovery rate using the Benjamini-Hochberg method. A false discovery rate <0.05 was considered significant. Motif analysis was conducted using MOMO (55) with a score-threshold of 1.0E-6.

Co-immunoprecipitation from cell culture extracts and mouse testes

PCDNA3.1-CMV-3XHA-HIPK4 and PCDNA3.1-CMV-3XFLAG-RIMBP3 plasmids were transfected into HEK293T cells using Lipofectamine 2000. Two days after transfection, the cells were lysed using Pierce IP Lysis Buffer (Thermo Fisher Scientific) supplemented with 1% protease inhibitor cocktail for 1 h at 4 °C and centrifuged at 12,000*g* for 30 min. The supernatant was removed and precleared using Protein A/G beads (Millipore) at 4 °C for 1 h. Mouse testicular lysates were prepared as described above. Subsequent experimental procedures were performed using the Pierce Co-Immunoprecipitation Kit (Thermo Scientific), and the eluted proteins were subjected to Western blotting.

Statistical analyses

All results are presented as the mean ± SD values. The statistical significance of the differences was determined using two-tailed Student's *t* test or one way ANOVA with Dunnett's *t* test. Each experiment was performed at least three times, and *p*-values <0.05 were considered significant.

Data availability

All MS raw files have been deposited to the PRIDE archive (https://www.ebi.ac.uk/pride/archive) and could be accessed with the dataset identifier PXD019303.

Supporting information—This article contains supporting information.

Acknowledgments—We would like to thank Dr Yarui Du and Guoliang Xu from SIBCB, CAS, for a kind gift of RIMBP3 antibodies.

Author contributions—X. G., J. Z., X. L., Y. G., and Z. H. methodology; X. G., J. Z., and Z. H. supervision; X. L., C. Z., Y. W., R. M., J. Z., Y. C., T. J., C. W., X. Y., C. S., and Y. G. investigation; X. L., T. J., C. W., C. Z., R. M., and Y. W. data curation; X. L., C. Z., R. M., and Y. W. writing-original draft; Y. C., Y. W., C. S., X. G., and Z. H. formal analysis; T. J., C. W., and X. Y. resources; X. G., J. Z., Z. H., X. L., C. Z., R. M., Y. C., Y. W., C. S., T. J., C. W., X. Y., and Y. G. writing-review and editing; X. L., C. Z., and Y. W. visualization; R. M. and Y. C. validation; Z. H., J. Z., and X. G. conceptualization; Z. H., J. Z., and X. G. project administration; Z. H., J. Z., and X. G. funding acquisition.

Funding and additional information—This work was supported by grants from the National Key R&D Program of China (2021YFC2700200) and National Natural Science Foundation of China (31530047, 31871445, 31501211, 81971439 and 32071133).

Conflict of interest—The authors declare no conflict of interest with contents of this article.

Abbreviations—The abbreviations used are: ES, ectoplasmic specialization; F-actin, filamentous actin; HIPK4, homeodomain-interacting protein kinase 4; NOA, nonobstructive azoospermia; OAT, oligoasthenoteratozoospermia; RIMBP3, RIMS-binding protein 3; TMT, tandem mass tags.

References

1. Irvine, D. S. (1998) Epidemiology and aetiology of male infertility. *Hum. Reprod.* **13 Suppl 1**, 33–44
2. Boivin, J., Bunting, L., Collins, J. A., and Nygren, K. G. (2007) International estimates of infertility prevalence and treatment-seeking: potential need and demand for infertility medical care. *Hum. Reprod.* **22**, 1506–1512
3. Sudhakar, D. V. S., Shah, R., and Gajbhiye, R. K. (2021) Genetics of male infertility - present and future: a narrative review. *J. Hum. Reprod. Sci.* **14**, 217–227
4. Jarow, J. P., Espeland, M. A., and Lipshultz, L. I. (1989) Evaluation of the azoospermic patient. *J. Urol.* **142**, 62–65
5. Matsumiya, K., Namiki, M., Takahara, S., Kondoh, N., Takada, S., Kiyohara, H., *et al.* (1994) Clinical study of azoospermia. *Int. J. Androl.* **17**, 140–142
6. Berookhim, B. M., and Schlegel, P. N. (2014) Azoospermia due to spermatogenic failure. *Urol. Clin. North Am.* **41**, 97–113
7. Lee, J. Y., Dada, R., Sabanegh, E., Carpi, A., and Agarwal, A. (2011) Role of genetics in azoospermia. *Urology* **77**, 598–601
8. Grootegoed, J. A., Baarends, W. M., Hendriksen, P. J., Hoogerbrugge, J. W., Slegtenhorst-Eegdeman, K. E., and Themmen, A. P. (1995) Molecular and cellular events in spermatogenesis. *Hum. Reprod.* **10 Suppl 1**, 10–14

9. Jan, S. Z., Hamer, G., Repping, S., de Rooij, D. G., van Pelt, A. M., and Vormer, T. L. (2012) Molecular control of rodent spermatogenesis. *Biochim. Biophys. Acta* **1822**, 1838–1850
10. Yan, W. (2009) Male infertility caused by spermiogenic defects: lessons from gene knockouts. *Mol. Cell. Endocrinol.* **306**, 24–32
11. O'Donnell, L. (2014) Mechanisms of spermiogenesis and spermiation and how they are disturbed. *Spermatogenesis* **4**, e979623
12. Sperry, A. O. (2012) The dynamic cytoskeleton of the developing male germ cell. *Biol. Cell* **104**, 297–305
13. O'Donnell, L., and O'Bryan, M. K. (2014) Microtubules and spermatogenesis. *Semin. Cell Dev. Biol.* **30**, 45–54
14. Lehti, M. S., and Sironen, A. (2016) Formation and function of the manchette and flagellum during spermatogenesis. *Reproduction* **151**, R43–R54
15. Pasch, E., Link, J., Beck, C., Scheuerle, S., and Alsheimer, M. (2015) The LINC complex component Sun4 plays a crucial role in sperm head formation and fertility. *Biol. Open* **4**, 1792–1802
16. Zhou, J., Du, Y. R., Qin, W. H., Hu, Y. G., Huang, Y. N., Bao, L., *et al.* (2009) RIM-BP3 is a manchette-associated protein essential for spermiogenesis. *Development* **136**, 373–382
17. Wang, Z., and Cole, P. A. (2014) Catalytic mechanisms and regulation of protein kinases. *Methods Enzymol.* **548**, 1–21
18. Wong, C. H., and Cheng, C. Y. (2005) Mitogen-activated protein kinases, adherens junction dynamics, and spermatogenesis: a review of recent data. *Dev. Biol.* **286**, 1–15
19. Qi, L., Liu, Z., Wang, J., Cui, Y., Guo, Y., Zhou, T., *et al.* (2014) Systematic analysis of the phosphoproteome and kinase-substrate networks in the mouse testis. *Mol. Cell. Proteomics* **13**, 3626–3638
20. Liu, X., Busby, J., John, C., Wei, J., Yuan, X., and Lu, M. L. (2013) Direct interaction between AR and PAK6 in androgen-stimulated PAK6 activation. *PLoS One* **8**, e77367
21. Kueng, P., Nikolova, Z., Djonov, V., Hemphill, A., Rohrbach, V., Boehlen, D., *et al.* (1997) A novel family of serine/threonine kinases participating in spermiogenesis. *J. Cell Biol.* **139**, 1851–1859
22. Zhao, H., Li, T., Zhao, Y., Tan, T., Liu, C., Liu, Y., *et al.* (2019) Single-cell transcriptomics of human oocytes: environment-driven metabolic competition and compensatory mechanisms during oocyte maturation. *Antioxid. Redox Signal.* **30**, 542–559
23. Ogurtsov, A. Y., Marino-Ramirez, L., Johnson, G. R., Landsman, D., Shabalina, S. A., and Spiridonov, N. A. (2008) Expression patterns of protein kinases correlate with gene architecture and evolutionary rates. *PLoS One* **3**, e3599
24. van der Laden, J., Soppa, U., and Becker, W. (2015) Effect of tyrosine autophosphorylation on catalytic activity and subcellular localisation of homeodomain-interacting protein kinases (HIPK). *Cell Commun. Signal.* **13**, 3
25. Guo, J., Grow, E. J., Mlcochova, H., Maher, G. J., Lindskog, C., Nie, X., *et al.* (2018) The adult human testis transcriptional cell atlas. *Cell Res.* **28**, 1141–1157
26. Wang, M., Liu, X., Chang, G., Chen, Y., An, G., Yan, L., *et al.* (2018) Single-cell RNA sequencing analysis reveals sequential cell fate transition during human spermatogenesis. *Cell Stem Cell* **23**, 599–614.e4
27. Crapster, J. A., Rack, P. G., Hellmann, Z. J., Le, A. D., Adams, C. M., Leib, R. D., *et al.* (2020) HIPK4 is essential for murine spermiogenesis. *Elife* **9**, e50209
28. Cheng, C. Y., and Mruk, D. D. (2010) A local autocrine axis in the testes that regulates spermatogenesis. *Nat. Rev. Endocrinol.* **6**, 380–395
29. Mruk, D. D., and Cheng, C. Y. (2004) Cell-cell interactions at the ectoplasmic specialization in the testis. *Trends Endocrinol. Metab.* **15**, 439–447
30. Vogl, A. W., Young, J. S., and Du, M. (2013) New insights into roles of tubulobulbar complexes in sperm release and turnover of blood-testis barrier. *Int. Rev. Cell Mol. Biol.* **303**, 319–355
31. Ubersax, J. A., and Ferrell, J. E., Jr. (2007) Mechanisms of specificity in protein phosphorylation. *Nat. Rev. Mol. Cell Biol.* **8**, 530–541
32. Cox, J., and Mann, M. (2008) MaxQuant enables high peptide identification rates, individualized p.p.b.-range mass accuracies and proteome-wide protein quantification. *Nat. Biotechnol.* **26**, 1367–1372
33. Schwartz, D., and Gygi, S. P. (2005) An iterative statistical approach to the identification of protein phosphorylation motifs from large-scale data sets. *Nat. Biotechnol.* **23**, 1391–1398
34. Ann, E. J., Kim, M. Y., Yoon, J. H., Ahn, J. S., Jo, E. H., Lee, H. J., *et al.* (2016) Tumor suppressor HIPK2 regulates malignant growth via phosphorylation of Notch1. *Cancer Res.* **76**, 4728–4740
35. Yamada, D., Perez-Torrado, R., Filion, G., Caly, M., Jammart, B., Devignot, V., *et al.* (2009) The human protein kinase HIPK2 phosphorylates and downregulates the methyl-binding transcription factor ZBTB4. *Oncogene* **28**, 2535–2544
36. de Kretser, D. M. (1997) Male infertility. *Lancet* **349**, 787–790
37. Don, J., and Stelzer, G. (2002) The expanding family of CREB/CREM transcription factors that are involved with spermatogenesis. *Mol. Cell. Endocrinol.* **187**, 115–124
38. Westlander, G. (2020) Utility of micro-TESE in the most severe cases of non-obstructive azoospermia. *Ups. J. Med. Sci.* **125**, 99–103
39. Cannarella, R., Condorelli, R. A., Duca, Y., La Vignera, S., and Calogero, A. E. (2019) New insights into the genetics of spermatogenic failure: a review of the literature. *Hum. Genet.* **138**, 125–140
40. Zafar, A., Eqani, S. A., Bostan, N., Cincinelli, A., Tahir, F., Shah, S. T., *et al.* (2015) Toxic metals signature in the human seminal plasma of Pakistani population and their potential role in male infertility. *Environ. Geochem. Health* **37**, 515–527
41. Alfano, M., Ferrarese, R., Locatelli, I., Ventimiglia, E., Ippolito, S., Gallina, P., *et al.* (2018) Testicular microbiome in azoospermic men-first evidence of the impact of an altered microenvironment. *Hum. Reprod.* **33**, 1212–1217
42. Cervan-Martin, M., Castilla, J. A., Palomino-Morales, R. J., and Carmona, F. D. (2020) Genetic landscape of nonobstructive azoospermia and new perspectives for the clinic. *J. Clin. Med.* **9**, 300
43. Ben Khelifa, M., Coutton, C., Zouari, R., Karaouzene, T., Rendu, J., Bidart, M., *et al.* (2014) Mutations in DNAH1, which encodes an inner arm heavy chain dynein, lead to male infertility from multiple morphological abnormalities of the sperm flagella. *Am. J. Hum. Genet.* **94**, 95–104
44. Neesen, J., Kirschner, R., Ochs, M., Schmiedl, A., Habermann, B., Mueller, C., *et al.* (2001) Disruption of an inner arm dynein heavy chain gene results in asthenozoospermia and reduced ciliary beat frequency. *Hum. Mol. Genet.* **10**, 1117–1128
45. Kierszenbaum, A. L., and Tres, L. L. (2004) The acrosome-acroplaxome-manchette complex and the shaping of the spermatid head. *Arch. Histol. Cytol.* **67**, 271–284
46. Russell, L. D., Russell, J. A., MacGregor, G. R., and Meistrich, M. L. (1991) Linkage of manchette microtubules to the nuclear envelope and observations of the role of the manchette in nuclear shaping during spermiogenesis in rodents. *Am. J. Anat.* **192**, 97–120
47. Mendoza-Lujambio, I., Burfeind, P., Dixkens, C., Meinhardt, A., Hoyer-Fender, S., Engel, W., *et al.* (2002) The Hook1 gene is non-functional in the abnormal spermatozoon head shape (azh) mutant mouse. *Hum. Mol. Genet.* **11**, 1647–1658
48. Kierszenbaum, A. L. (2002) Intramanchette transport (IMT): managing the making of the spermatid head, centrosome, and tail. *Mol. Reprod. Dev.* **63**, 1–4
49. Alonso, A., Sasin, J., Bottini, N., Friedberg, I., Friedberg, I., Osterman, A., *et al.* (2004) Protein tyrosine phosphatases in the human genome. *Cell* **117**, 699–711
50. Cooper, T. G., Noonan, E., von Eckardstein, S., Auger, J., Baker, H. W., Behre, H. M., *et al.* (2010) World Health Organization reference values for human semen characteristics. *Hum. Reprod. Update* **16**, 231–245
51. Wang, D., Cheng, L., Xia, W., Liu, X., Guo, Y., Yang, X., *et al.* (2020) LYPD4, mouse homolog of a human acrosome protein, is essential for sperm fertilizing ability and male fertilitydagger. *Biol. Reprod.* **102**, 1033–1044
52. Tyanova, S., Temu, T., and Cox, J. (2016) The MaxQuant computational platform for mass spectrometry-based shotgun proteomics. *Nat. Protoc.* **11**, 2301–2319
53. Yu, G., Wang, L. G., Han, Y., and He, Q. Y. (2012) clusterProfiler: an R package for comparing biological themes among gene clusters. *OMICS* **16**, 284–287
54. Shannon, P., Markiel, A., Ozier, O., Baliga, N. S., Wang, J. T., Ramage, D., *et al.* (2003) Cytoscape: a software environment for integrated models of biomolecular interaction networks. *Genome Res.* **13**, 2498–2504
55. Cheng, A., Grant, C. E., Noble, W. S., and Bailey, T. L. (2019) MoMo: discovery of statistically significant post-translational modification motifs. *Bioinformatics* **35**, 2774–2782